Available online at www.sciencedirect.com
SCIENCE DIRECT®
Agricultural and Forest Meteorology 130 (2005) 39–58
AGRICULTURAL AND FOREST METEOROLOGY
www.elsevier.com/locate/agrformet

Vertical stratification of soil water storage and release dynamics in Pacific Northwest coniferous forests

J.M. Warren [a,*], F.C. Meinzer [a], J.R. Brooks [b], J.C. Domec [c]

[a] USDA Forest Service, PNW Research Station, 3200 SW Jefferson Way, Corvallis, OR 97331, USA
[b] Western Ecology Division, US EPA/NHEERL, Corvallis, OR 97333 USA
[c] Department of Wood Science and Engineering, Oregon State University, Corvallis, OR 97331, USA

Received 21 July 2004; accepted 31 January 2005

Abstract

We characterized vertical variation in the seasonal release of stored soil moisture in old-growth ponderosa pine (OG-PP, xeric), and young and old-growth Douglas-fir (Y-DF, OG-DF, mesic) forests to evaluate changes in water availability for root uptake. Soil water potential (ψ) and volumetric water content (θ) were measured concurrently at 10 cm intervals to 1 m depth to create in situ soil water retention curves (SWRC) under drying conditions. Non-linear regression was used to fit SWRC specific to each depth and site. We also quantified root biomass, soil texture, and hydraulic redistribution (HR) of soil water by roots to identify factors affecting the seasonal dynamics of root water uptake and depletion from the soil profile. Soil θ measured at a particular ψ increased with soil depth, and was strongly dependent upon soil texture. For example, when ψ was -0.1 MPa, θ ranged from 13% at 20 cm to 35% at 100 cm for the OG-DF forest. Soil texture and bulk density accounted for 60–90% of the variation in the SWRC. As the summer drought progressed, water extraction shifted to the deeper layers, and recharge from HR approached 0.15 mm day^{-1} in the upper 60 cm for all sites. Total water use from the upper 2 m at all sites peaked between 1.5–2.5 mm day^{-1} in mid-July and then declined to 0.5–1.0 mm day^{-1} by the end of the dry season. Total fine root biomass in the upper 1 m was 0.77 kg m^{-2} (OG-PP), 1.08 kg m^{-2} (OG-DF) and 1.15 kg m^{-2} (Y-DF), with 40% (PP) to 60% (DF) of fine roots located in the upper 20 cm. However, the upper 20 cm only accounted for 20% of total water depletion from the upper 2 m at peak water uptake, declining to 4–6% later in the season, illustrating the contribution of deeper roots to water uptake. Nevertheless, daily water uptake from the entire 2 m profile was strongly dependent on water potential at 20 cm, indicating that fine roots in the upper soil may play an important role in regulating water uptake through hydraulic effects on stomatal conductance.

Keywords: Root water uptake; Soil water modeling; Water retention curve; Hydraulic redistribution; Water potential; Volumetric water content; Douglas-fir; Ponderosa pine

1. Introduction

Plant communities that experience low precipitation inputs during the growing season must rely on

* Corresponding author. Tel.: +1 541 758 8766; fax: +1 541 750 7329.
E-mail address: jeffwarren@fs.fed.us (J.M. Warren).

0168-1923/$ – see front matter © 2005 Elsevier B.V. All rights reserved.
doi:10.1016/j.agrformet.2005.01.004

plant or soil water storage to provide adequate water for growth processes. The uptake of stored soil water by roots depends on soil physical and chemical characteristics and is driven by water potential gradients within the soil-plant-atmosphere continuum. The dynamics of soil water storage and release (uptake) from the unsaturated vadose zone govern various aspects of ecosystem functioning. A good understanding of soil water dynamics is therefore, critical for modeling water and heat flux, plant productivity and stand development. However, belowground processes are technically more difficult to quantify than aboveground processes due to the much denser and arguably more heterogeneous soil medium. As such, in situ physical and physiological data from belowground observations for use in modeling water and carbon dynamics through ecosystems are relatively scarce, which often necessitates a simplified 'black box' style treatment of some processes.

Soil water release under drying conditions is site- and depth-specific, and is non-linearly related to soil water potential (Brooks and Corey, 1964; van Genuchten, 1980). Measurement of soil water content (θ) and soil water potential (ψ) in the field is expensive, time consuming and technically difficult and thus datasets containing concurrent in situ measurements of θ and ψ are scarce (e.g., Bréda et al., 1995; Katul et al., 1997). Soil water retention curves (SWRC) relating θ and ψ are more frequently generated by progressively drying soil cores in the lab where θ and ψ are easily measured gravimetrically (θ) or with pressure plates (ψ) (e.g., Abrahamson et al., 1998; Heiskanen and Mäkitalo, 2002). Another alternative is to measure soil physical characteristics, such as soil texture, bulk density (BD) or organic matter, which affect the release of stored water under drying conditions in a predictable manner. Soil particle size distribution (sand, silt, and clay (%)) and/or other soil characteristics can be substituted into pedotransfer functions (Saxton et al., 1986; Wösten et al., 2001) to generate SWRC that relate water content to water potential (Brooks and Corey, 1964; van Genuchten, 1980). Related equations can also be used to estimate unsaturated soil hydraulic conductivity if saturated conductivity is known (Mualem, 1976; van Genuchten, 1980). Thus, in principle, the general dynamics of soil water movement and release can be estimated using only a few simple equations. However, comparisons with empirical in situ data to test the validity of this approach are rare.

It has been widely reported that water uptake and growth of shallowly-rooted herbaceous crops and grasses falls precipitously as ψ declines (e.g., Yang and de Jong, 1971; Childs and Hanks, 1975; Schleiff and Schaffer, 1984; Zhang and Davies, 1989; Dean-Knox et al., 1998). However, few field studies have described the dependence of water uptake by woody roots on ψ in forest vegetation that experiences prolonged seasonal drought (e.g., Bréda et al., 1995). In coniferous forests of the Pacific Northwest, for example, water potential in the upper soil horizons commonly falls below -1.5 MPa during the dry summer months (Meinzer et al., 2004; Domec et al., 2004), yet forest transpiration is sustained at relatively high rates (Irvine et al., 2002). This implies that shallow roots of coniferous trees are able to continue extracting soil water at very low water potentials or that a substantial fraction of transpired water is taken up by deep roots located in horizons where ψ is closer to zero. Predawn leaf water potential has routinely been used as a surrogate for ψ (e.g., Law et al., 2000b), but several recent reports indicate that substantial predawn disequilibrium between plant and ψ can exist owing to factors such as nocturnal transpiration and hydraulic redistribution, especially for ecosystems that experience extended dry seasons (e.g., Donovan et al., 2003; Bucci et al., 2004). Thus, the most reliable way to evaluate ψ and its impact on root water uptake is to either measure it directly, or to validate models that predict ψ from soil physical characteristics and the more easily measured θ.

In the present study, we characterized vertical gradients in θ, ψ, and the underlying soil physical and biological characteristics for three contrasting coniferous forest ecosystems in Oregon and Washington, USA during a seasonal dry period. These measurements allowed us to evaluate the range of physiologically available soil water storage, the effect of hydraulic redistribution on θ, ψ, and vertical gradients in soil water release characteristics. The semiarid ponderosa pine ecosystem and two mesic Douglas-fir ecosystems studied have been extensively investigated and some of their key processes modeled over the past several years (Law et al., 2000a,b; Phillips et al., 2002; Licata, 2003; Unsworth et al., 2004; Chen et al., 2004). Our goals were to create site-specific in situ SWRC

that are critical for understanding and modeling hydrologic dynamics in these ecosystems, and to evaluate differences and similarities among sites in vertical stratification of water uptake by roots and its dependence on ψ.

2. Materials and methods

2.1. Site descriptions

This study is part of a broader investigation focusing on soil-plant-atmosphere water dynamics in different Pacific Northwest coniferous forest ecosystems (Brooks et al., in review; Meinzer et al., 2004; Domec et al., 2004). Data for the present study were collected from a young Douglas-fir stand (Y-DF), an old-growth mixed Douglas-fir/Hemlock stand (OG-DF), and an old-growth ponderosa pine stand (OG-PP) during the 2002 seasonal dry period. Average annual precipitation at the Douglas-fir sites exceeds 2200 mm, while the relatively dry ponderosa pine site receives just 550 mm of precipitation annually. All three sites experience a prolonged seasonal drought between late spring and early fall. Additional climate and stand characteristics are described in Table 1.

The young and old-growth Douglas-fir stands were located at or near the Wind River Canopy Crane Research Facility (WRCCRF) within the Gifford Pinchot National Forest southeast of Mount Saint Helens in south central Washington, USA (45°49′N, 121°57′W), at elevations of 560 and 370 m, respectively. The Y-DF stand was located in the Wind River Experimental Forest about 5 km from the WRCCRF, and was a 24-year-old plantation established on previously logged land. The upper canopy consisted primarily of Douglas-fir (*Pseudotsuga menziesii* (Mirb.) Franco), with vine maple (*Acer circinatum*

Table 1
Site climatic and stand characteristics for the young and old-growth Douglas-fir stands, and for the old-growth pine stand

	Y-DF	OG-DF	OG-PP
Length of dry season (months)	3–4	3–4	5–6
Precipitation[a,b] (mm)			
Annual	2200	2200	550
Dry season (2002)	46 (Jul 1–Nov 1)	46 (Jul 1–Nov 1)	18 (May 1–Nov 1)
Drought (2002)	4 (Jul 19–Sep 7)	4 (Jul 19–Sep 7)	7 (Jun 9–Sep 27)
Temperature[b,c] (°C)			
Dry season mean	17	17	14
Mean daily maximum	25	25	25
Maximum diel range	25	25	24
Soil water content @ 20 cm ($m^3\ m^{-3}$)			
Start of dry season	0.22	0.18	0.12
End of dry season	0.12	0.10	0.05
Leaf area index[d,e] ($m^2\ m^{-2}$)	11	9	2.1
Stand density[a,e,f,g] (trees ha^{-1})	1529	427	555/72 (50/250-year-old)
Basal area[a,f] ($m^2\ ha^{-1}$)	48	83	30
Canopy height[a,d,h] (m)			
Mean	16	19	10/34 (50/250-year-old)
Maximum	20	65	42

[a] Shaw et al. (2004).
[b] B. Law (personal communication).
[c] Wind River Canopy Crane Research Facility online database: http://depts.washington.edu/wrccrf/database.html.
[d] Irvine and Law (2002).
[e] Phillips et al. (2002).
[f] Law et al. (2001).
[g] D. Woodruff (personal communication).
[h] Ryan et al. (2000).

5Pursh.) in the sub-canopy, and huckleberry (*Vaccinium* spp.), Oregon-grape (*Berberis nervosa* Pursh.), and western hemlock (*Tsuga heterophylla* (Raf.) Sarg.) regeneration in the understory. The OG-DF stand was approximately 450 years old, and was established after a stand-clearing fire. Douglas-fir and western hemlock were the dominant species, with some western red cedar (*Thuja plicata* Donn ex D. Don) and true firs (*Abies* spp.) sharing the canopy. The mid-canopy consisted of Pacific silver fir (*Abies amabilis* Dougl. ex Forbes) and Pacific yew (*Taxus brevifolia* Nutt.) and the understory was dominated by vine maple, salal (*Gaultheria shallon* Pursh.) and Oregon-grape (Shaw et al., 2004).

Soils at the Y-DF and OG-DF sites have been classified as medial, mesic, and Entic Vitrands (Klopatek, 2002; Shaw et al., 2004). These are deep, well-drained Andisols containing large amounts of volcanic tephra in the upper profile. The mineral soil transitions from a sandy loam in the upper soil to a clay loam in the subsoil (Shaw et al., 2004). There was a well-developed organic mull layer above the mineral soil at both sites, 4.1 ± 1.1 cm deep for the Y-DF site ($n = 8$; range 0–8 cm), and 5.8 ± 1.3 cm deep for the OG-DF site ($n = 8$; range 3–14 cm). This organic layer contained soil carbon (C) concentrations >400 g kg^{-1} (Klopatek, 2002). Soil C in the upper 20 cm of mineral soil ranged from 73–43 g kg^{-1}, for the Y-DF and OG-DF sites, respectively, (Klopatek, 2002). The water table at these sites varies seasonally, and is often less than 2 m below the surface during the wet season at the OG-DF site (Shaw et al., 2004). Water remained physiologically available at or above 2 m throughout the dry season (Brooks et al., 2002; Meinzer et al., 2004). Douglas-fir roots have been observed at these sites at depths of at least 2 m (J. Licata, T. Hinckley, personal communication).

The old-growth ponderosa pine stand was located within the Metolius Research Natural Area within the Deschutes National Forest in the rain-shadow east of the Cascade Mountains in central Oregon, USA (44°30′ N, 121°37′ W) at an elevation of 915 m. The OG-PP stand was a relatively open pine savanna primarily comprised of ponderosa pine (*Pinus ponderosa* Dougl. ex Laws.). The overstory contained 250–300-year-old dominant trees, a large cohort of ~50-year-old suppressed trees, and mixed-age trees <100-year-old (Law et al., 2000a; Ryan et al., 2000). There was a sparse understory dominated by bracken fern (*Pteridium aquilimum* (L.) Kuhn), bitterbrush (*Purshia tridentata* (Pursh) DC), and wild strawberry (*Fragaria vesca* L.). Pine regeneration consisted of small groups of stunted seedlings, almost exclusively <20 cm tall.

Soil at the OG-PP site has been classified as an Alfic Vitrixerand, consisting of 73% sand, 21% silt, and 6% clay in the upper 100 cm (Law et al., 1999, 2001a,b). There was a distinct organic soil layer (3.6 ± 0.6 cm deep; range 0–5 cm) between the pine litter layer and mineral soil. The mineral soils were relatively low in organic matter, with C concentrations ranging from 13 g kg^{-1} at 20 cm to 6 g kg^{-1} at 100 cm (Law et al., 2001a,b). The water table was below 2.5 m at the OG-PP site during the study period based on observations collected during previous equipment installation (Brooks et al., 2002). Rooting depth has been estimated to be >3 m based on wind thrown trees (Ryan et al., 2000).

2.2. Sap flow

Stem sap flow was measured throughout the 2002 dry season in large pine ($n = 3$), Douglas-fir ($n = 4$), and hemlock ($n = 3$) trees with uniform stems and crowns at the two old-growth sites to provide a relative measure of tree water use. Sap flow was not quantified for trees at the young Douglas-fir site. Four or five sets of variable-length thermal dissipation sensors (James et al., 2002) were installed into the stem sapwood of each tree at a height of 2 m. For this study, only data from the outer sensors (~2 cm) were used, which provided a relative index of tree water use across the season. Each pair of sensors consisted of a heated and unheated probe containing thermocouples. The sensors were protected against thermal gradients and precipitation by reflective insulation. Temperature differences between sensors were scanned every minute and averages were recorded every 10 min using a datalogger (CR10X, Campbell Scientific, Logon, UT, USA), then converted to sap flow density using the empirical calibration of Granier (1985) confirmed by Clearwater et al. (1999).

2.3. Soil water potential

Soil water potentials, ψ, were quantified using thermocouple psychrometers (PST-55, Wescor,

Logan, UT) installed at depths of 20, 30, 40, 50, 60, and 100 cm. The psychrometers measure the combined soil matric and osmotic potentials. For some soil types (especially saline or agricultural soils), the osmotic potential can make up a significant portion of the total ψ (e.g., Schleiff and Schaffer, 1984; Dean-Knox et al., 1998) and may become a larger component of ψ under drying conditions. Prior to installation, the psychrometers were individually calibrated in the laboratory against salt solutions of known osmolality (Brown and Bartos, 1982). A soil auger was used to excavate 1 m deep holes, and psychrometers were placed into the intact soil profile in the side of the hole at each depth to reduce installation artifacts. Four replicates were spaced out across a representative 25 m^2 area at each site. Water potentials were measured every 30 min, with a 30 s cooling time to accommodate the Peltier effect and data were recorded by a datalogger (CR-7, Campbell Scientific, Logan, UT, USA). Sheaths of reflective insulation were secured around exposed psychrometer cables and data logger to minimize temperature gradients within the cable and logger that could influence water potential calculations.

2.4. Soil volumetric water content

Soil volumetric water content, θ, was quantified using multi-sensor, frequency domain capacitance probes (Paltineanu and Starr, 1997; Brooks et al., 2002). These probes contained eight annular capacitance sensors (EnviroSCAN, Sentek Pty Ltd., Adelaide, Australia) capable of quantifying minute changes in θ (±0.003%). Each probe was installed into a ~6 cm diameter PVC access tube, to a depth of 2 m, with sensors spaced at 20, 30, 40, 50, 60, 100, 150, and 200 cm depths. The sensors measured changes in the soil dielectric constant across a ~10 cm × 10 cm sphere of influence surrounding the sensor, and thus integrated across all components of the soil profile, including roots and rocks. Water content was estimated based on applying a calibration equation to the scaled frequency output of the capacitance sensors. A default factory calibration equation based on average soils was supplied; however, each specific soil type was unique and required field calibration to determine absolute values of θ (described below). Volumetric water content was measured every 10 min and recorded by a datalogger (model RT6, Sentek Pty Ltd., Adelaide, Australia). Four replicate capacitance probes were located in the vicinity of the four psychrometer arrays to provide concurrent measurements at similar locations.

Each capacitance sensor was frequency-normalized by calibration against air and water in the laboratory to ensure the precision of measurements. Field-based calibration to the specific sandy loam soils of the Pacific Northwest was necessary to ensure the accuracy of measurements (Morgan et al., 1999). In the field, two soil cores were extracted with a 409 cm^3 volumetric auger 0.5 m away from each capacitance probe at three depths (10–30, 30–50, and 50–70 cm), sealed in plastic bags and taken to the laboratory to determine wet (field) and oven-dry mass. Careful measurements were made so that the exact volume of soil removed for each sampling depth was known. Volumetric soil water content of each core was calculated by the difference between wet and dry mass divided by the known volume. Volumetric water contents ($\theta_{measured}$) were compared to concurrent capacitance sensor-based water contents (θ_{sensor}) derived using the factory-supplied default calibration. Data from all sites were pooled together which resulted in a wide ambient range of water contents (0.06–0.33 $m^3\ m^{-3}$). A linear regression was generated to relate $\theta_{measured}$ to θ_{sensor}:

$$\theta_{sensor} = 0.84 \pm 0.037 \times \theta_{measured} - 1.1 \pm 0.21 \quad (n = 29; R^2 = 0.95) \tag{1}$$

This relationship was used to generate a new calibration equation to convert the scaled frequency output of the capacitance sensors to actual volumetric water content:

$$\theta = \left(\frac{SF + 0.1299}{0.2727}\right)^{2.939} \tag{2}$$

where SF is the scaled frequency of an individual capacitance sensor based on its frequency output in air (F_a), water (F_w), and the soil (F_s):

$$SF = \frac{F_a - F_s}{F_a - F_w} \tag{3}$$

The three constants in Eq. (2) can be used to create a new calibration equation within the EnviroSCAN software program which can be applied to the SF data for analysis. It should be noted that the accuracy of the

θ calibration was limited to three significant digits based on the regression (Eq. (1)); e.g., 10.1%. Relative precision of θ measurements was limited only by the sensor itself; e.g., $10.125 \pm 0.002\%$, and could be used to quantify small diel fluctuations in θ in the vicinity of a single sensor.

2.5. Seasonal water use

Estimates of seasonal water use were based on patterns of θ in the upper 2 m of soil. Water use was based on differences in daily minimum θ and maximum θ for each sensor at each depth. Monthly mean values were integrated across depth to generate mean daily water depletion from the upper 2 m. At the OG-PP site, data were compared with total site evapotranspiration (ET) based on eddy covariance measurements of water vapor flux from a 47 m tower (Law et al., 2000a; Anthoni et al., 2002).

2.6. Hydraulic redistribution

Hydraulic redistribution (HR) of soil water (Richards and Caldwell, 1987) was calculated based on diel fluctuations in θ within each soil layer (Brooks et al., 2002). Soil water content declined during the day when tree and root demand were highest. At night, θ increased in the upper soil layers as water was moved via roots from wetter soil layers to drier soil layers following a water potential gradient. This nighttime increase in θ in the absence of precipitation was considered to be HR: $\mathrm{HR} = \theta_{\max}\ (\text{day } x+1) - \theta_{\min}\ (\text{day } x)$. The magnitude of daily HR was estimated for each sensor and then integrated across the profile to provide total daily HR within the 15–60 cm soil layer.

2.7. Soil water retention curves

Soil ψ and θ were measured concurrently within 1 m of each other at four locations in each site during the seasonal dry-down. Mean daily values of ψ and θ were used to generate SWRC for each depth and site. Data used for the SWRC were collected during 50 or 110 day droughts at the Douglas-fir and pine sites respectively (Table 1). Soil ψ and θ data were screened for outlying values, which were removed from the subsequent curve-analyses. A curve-fitting program (Sigma Plot 7.101, SPSS Inc., Chicago, IL) was used to fit a simple three-parameter non-linear regression curve to the data at each depth:

$$\psi = \frac{-1}{(a + b\theta)^c} \tag{4}$$

where a, b, c are parameters determined by the regression. Other less complex exponential rise to maximum curves (e.g., $\psi = a\theta^{-b}$) did not adequately fit the data, particularly for $\psi > -0.2$ MPa. Data from different depths were pooled together into a single SWRC when the data sets overlapped completely throughout the measurement range. Alternate groups of curves spanning other depth ranges were generated for comparison across sites. In addition, the data were fit to the four-parameter soil water retention model of Brooks and Corey (1964):

$$\frac{\theta - \theta_\mathrm{r}}{\theta_\mathrm{s} - \theta_\mathrm{r}} = \left(\frac{\psi_\mathrm{cr}}{\psi}\right)^{\lambda} \quad \text{for } \psi < \psi_\mathrm{cr} \tag{5}$$

where θ_s is the saturated soil volumetric water content, θ_r is the residual soil volumetric water content (for very dry soil), ψ_cr is the soil water potential as θ approaches saturation, and λ is a parameter related to soil porosity (texture). This function can be solved for ψ:

$$\psi = \psi_\mathrm{cr}\left(\frac{\theta_\mathrm{r} - \theta}{\theta_\mathrm{r} - \theta_\mathrm{s}}\right)^{1/\lambda} \tag{6}$$

The regression program used an iterative least squares method to evaluate the best fit for each dependent parameter based on initial estimates of θ_s and θ_r. Estimates of θ_s were generated from in situ field measurements of θ in early spring prior to the seasonal dry down, or after late autumn rains had recharged the soil. Maximum values of θ_s were sampled from each soil depth at least 24 h after a precipitation pulse moved through the profile. Values of θ_r were estimated by trial and error, inputting θ_s and various estimates of θ_r ($0 < \theta_\mathrm{r} < \theta_\mathrm{s}$) into the model to maximize the t-test statistics to best predict the dependent parameters ψ_cr and λ. Only 5–10 representative measured data points and error bars were included in the SWRC figures for clarity, except for the inset figure, which contains daily data points used in the regression and all vertical error bars for ψ, but only several representative error bars for θ.

2.8. Soil and root analyses

Soil cores were collected at each site using a custom-built soil auger fitted with a 5.1 cm hole-saw. Cores ($n = 8$, 1 m depth) were taken just below the litter layer at distances ranging from 1–6 m from the dominant canopy trees. Cores were sectioned by depth (0–20, 20–40, 40–60, 60–80, and 80–100 cm) and the samples sealed in plastic bags for later analysis. The upper 20 cm profile was additionally partitioned into the organic and mineral horizons. Soil samples were kept at 4 °C until roots could be separated and analyzed. Roots, large organic material and coarse debris were removed from the soil samples by passing soil through a 2.0 mm mesh screen. Roots and soil samples were retained for analysis.

Particle size distribution was estimated for soil samples from each depth using the hydrometer method (Gee and Bauder, 1986). In addition, the analysis included several soil samples collected at the OG-DF site at depths up to 2.5 m. Screened soil was dried at 30 °C, and the percentages of sand (2.0–0.05 mm), silt (0.05–0.002 mm) and clay (<0.002 mm) were determined ($n = 6$ for Y-DF and OG-PP, $n = 8$ for OG-DF) based on time-course changes in specific gravity of liquid-suspended samples. The USDA Textural Classification system was used to assign a textural class to each sample. Particle size analysis was performed by the Soil Science Physical Characterization Lab within the Department of Crop and Soil Science at Oregon State University. Internal soil standards provided a measure of variability within the analyses.

Sieved root samples ($n = 8$) were manually separated from the remaining soil material using tweezers and a hand lens. Root material was washed in distilled water and separated into three size classes: fine roots (<2 mm), medium roots (2–5 mm), and coarse roots (>5 mm). Visibly dead, decaying roots were removed. There was no distinction made between roots of different woody species. Projected root surface area images were generated by scanning roots with a computer scanner (model 5400c, Hewlett-Packard Co., Palo Alto, CA, USA). Public domain java image processing software (ImageJ, Research Services Branch, National Institute of Mental Health, Bethesda, MD, USA) was used to determine the number of data-containing pixels in each image, resulting in a relative projected root surface area for each image. Projected root surface area was adjusted by π to achieve total root surface area, based on the assumption that root cross-sections were circular. The scanner and software were calibrated using known areas of dark paper cut into small root-shaped segments. A calibration curve was generated that related pixel number to actual area (Sigma Plot 7.101, SPSS Inc., Chicago, IL). Roots were dried at 60 °C to constant mass for biomass determination.

Saturated soil hydraulic conductivity (K_s) was estimated for the upper soil layers using a computer program based on hierarchical pedotransfer functions (Schaap et al., 2001; ROSETTA version 1.2, US Salinity Laboratory ARS-USDA, Riverside, CA, USA). Input parameters included measured soil texture (sand, silt, clay (%)), BD and θ at −0.03 MPa. In addition, the model could use θ at −1.50 MPa if available, in this case only for soil at the OG-PP site <40 cm deep. Values used for BD were 0.83, 0.89, and 0.98 g cm^{-3} (Y-DF), 0.81, 0.79, and 0.78 g cm^{-3} (OG-DF) and 1.00, 1.04, and 1.18 g cm^{-3} (OG-PP) for depths 0–20, 20–40, and 40–60, respectively. Estimates of K_s based solely on soil texture were included for comparison.

2.9. Statistical analyses

Multiple linear regression techniques were used to relate physical and biological characteristics of the soil to the modeled SWRC (Eq. (4)) to generate pedotransfer functions. Four models were used to relate depth-dependent changes in θ at a specific ψ (−0.1 or −0.75 MPa):

(A) $\theta = \alpha + \beta_1$ sand + β_2 silt + β_3 clay + ε
(B) $\theta = \alpha + \beta_1$ sand + β_2 silt + β_3 clay + β_4 bulk density (BD) + ε
(C) $\theta = \alpha + \beta_1$ sand + β_2 silt + β_3 clay + β_4 root surface area (SA_{root}) + ε
(D) $\theta = \alpha + \beta_1$ sand + β_2 silt + β_3 clay + β_4 BD + β_5 SA_{root} + ε

In the models α is the intercept, β_1, β_2, β_3, β_4, and β_5 are the partial regression coefficients and ε represents the error term. Missing BD and θ (at $\psi = -0.75$ MPa) at 100 cm depth reduced the sample size for some of the regressions. Models used the best-fit adjusted R^2 selection technique and included the Bayesian infor-

mation criterion statistic (BIC) to compare different models. Higher absolute values of BIC indicate a better regression model.

Pearson correlation coefficients were produced for each parameter considered to affect the SWRC to describe relationships between variables and to justify the regression models. Correlations were considered to be significant at $P \leq 0.05$ ($n = 11$–13)

One and two-way analysis of variance (ANOVA), including post-hoc tests when necessary, were conducted on each of the quantified physical or biological characteristics to measure significant differences between and within soil layers, between sites, and across sites. Appropriate error terms were used for the two-way ANOVA. Differences were considered significant at $P \leq 0.05$. All statistical analyses were conducted using SAS statistical software (Version 8.02, SAS Institute Inc., Cary, NC, USA).

3. Results

Root water uptake combined with the absence of precipitation during the summer drought generated ψ gradients within the soil–plant system that acted as a driving force for water movement. The declining θ during the drought was non-linearly related to changes in soil ψ (Fig. 1). Early in the season when the soil was close to field capacity, large declines in θ resulted in relatively small declines in ψ (Fig. 1). As the soils dried out, relatively small declines in θ resulted in increasingly large declines in soil ψ, reflecting the diminishing availability of unbound water. During the summer drought, soil ψ at 20 cm reached −2.2 MPa at the OG-PP site, lower than at the Y-DF (−1.2 MPa) or OG-DF (−0.8 MPa) sites (Fig. 1). The decline in ψ in the upper soil resulted from significant depletion of retained soil water, with θ approaching 0.11, 0.10, or 0.05 $m^3\ m^{-3}$ at the end of the drought for the Y-DF, OG-DF, and OG-PP sites, respectively (Fig. 1, Table 1). There was significant spatial and temporal variation in θ and ψ at each specific depth within a site due to the heterogeneity of the soil medium. In general, θ was spatially more variable early in the season when the soils were relatively moist, and then stabilized as seasonal minimum values of θ were reached. In contrast, ψ was stable early in the season, and then became increasingly variable during a transitional phase in the SWRC (approximately $-0.20 < \psi < -0.01$) when soils began to rapidly dry out (see Fig. 1, inset). Temporally non-uniform local soil drying near the ψ sensors resulted in the

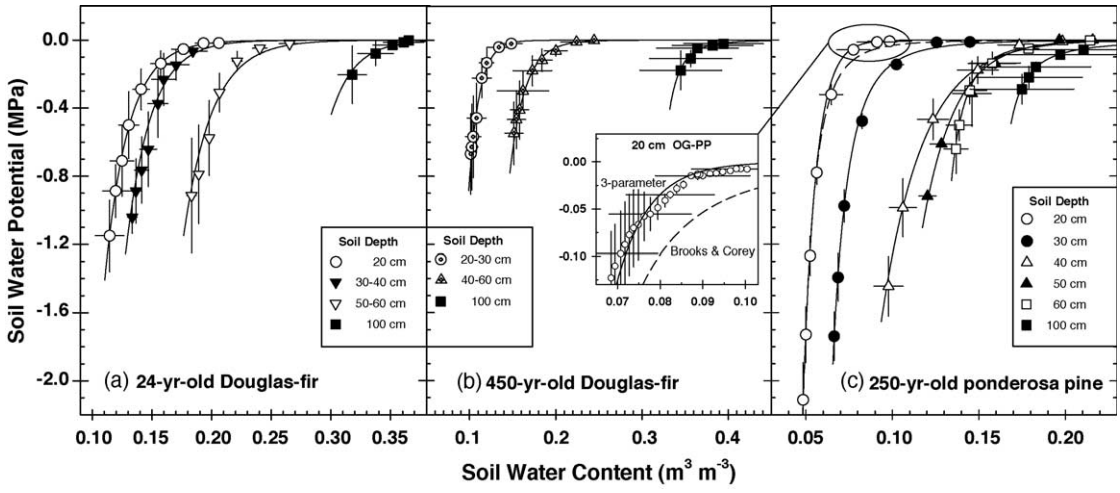

Fig. 1. Soil water retention curves generated in situ for young- and old-growth Douglas-fir stands and for an old-growth ponderosa pine stand during the seasonal drought in 2002. Curves were based upon 50 or 110 days of concurrent soil water potential and soil water content measurements using 3–4 sensors per depth, for Douglas-fir or pine stands, respectively. Vertical or horizontal bars represent the standard error. Similar curves from adjacent depths were combined when data overlapped completely throughout the measurement range. A three parameter model ($\psi = -(a + b\theta)^{-c}$) was fit to the data. The inset figure contrasts the three-parameter model (solid line) with the four-parameter model of Brooks and Corey (1964) (dashed line).

Table 2
Soil water retention curve-fitting parameters from young and old Douglas-fir, and old ponderosa pine ecosystems

Site description	Soil depth	n	Three parameter model			Brooks and Corey model			
			a	b	c	θ_s	θ_r	Ψ_{cr}	λ
Douglas-fir: 24-year-old plantation	20	42	9.48E−01	4.44E−01	1.13E+02	0.24	0.055	−2.07E−02	2.82E−01
	30–40	40	9.67E−01	2.49E−01	1.95E+02	0.30	0.080	−1.22E−02	3.15E − 01
	50–60	42	9.68E−01	1.78E−01	2.35E+02	0.36	0.130	−1.65E−02	3.59E−01
	100	31	9.31E−01	2.43E−01	2.10E+02	0.44	0.240	−2.81E−03	2.23E−01
	20–30	35	9.59E−01	3.29E−01	1.48E+02	0.26	0.065	−1.80E−02	2.91E − 01
	40–60	32	9.68E−01	1.91E−01	2.35E+02	0.33	0.105	−1.33E−02	2.99E − 01
Douglas-fir: 450-year-old mixed conifer	20–30	29	9.60E−01	4.10E−01	1.99E+02	0.22	0.055	−2.41E−03	2.23E−01
	40–60	36	7.08E−01	2.05E+00	2.80E+01	0.33	0.095	−1.59E−03	2.35E−01
	100	51	−6.53E+00	2.34E+01	4.11E+00	0.50	0.165	−3.10E−04	9.80E−02
Ponderosa pine: 300-year-old pine savanna	20	107	9.33E−01	1.24E+00	1.07E+02	0.17	0.025	−2.92E−03	2.76E−01
	30	111	−8.77E−01	2.61E+01	3.57E+00	0.21	0.035	−4.73E−03	2.91E−01
	40	105	9.72E−01	2.65E−01	1.57E+02	0.28	0.035	−1.73E−02	3.03E−01
	50	81	9.61E−01	3.27E−01	1.62E+02	0.31	0.035	−2.20E−03	1.93E−01
	60	71	−5.33E+00	4.77E+01	2.76E+00	0.31	0.105	−1.27E−03	3.02E−01
	100	65	−1.41E+01	9.25E+01	1.76E+00	0.31	0.150	−8.05E−03	5.21E−01
	20–30	44	7.80E−01	3.49E+00	3.30E+01	0.19	0.015	−9.20E−04	1.85E−01
	40–60	24	9.63E−01	3.13E−01	1.81E+02	0.30	0.060	−1.52E−03	2.09E−01

A three-parameter function: $\Psi_{soil} = \frac{-1}{(a+b\theta_{soil})^c}$ provided the best fit, although the four-parameter function of Brooks and Corey (1964): $\Psi = \Psi_{cr}\left(\frac{\theta_r-\theta}{\theta_r-\theta_s}\right)^{1/\lambda}$ provided an adequate fit (see Fig. 1), and included soil moisture parameters for saturated and residual volumetric water content (θ_s and θ_r), near-saturated water potential (ψ_{cr}) and a parameter related to texture (λ). Data from different depths were pooled together when their data overlapped completely throughout the measurement range. Additional groupings were provided for comparison across sites.

increasing ψ variability depicted in the transitional phase of the SWRC (Fig. 1).

SWRC varied with depth at each site (Fig. 1, Table 2). Data collected from the six depths fell along four curves at the Y-DF site, three curves at the OG-DF site and six curves at the OG-PP site. Data from the 40, 50, and 60 cm depths at OG-PP followed the same curve initially (0 to −0.2 MPa), then began to diverge so that by the end of the dry season they were clearly unique (Fig. 1). The two equations used to fit the SWRC yielded different results (Fig. 1, inset). Although both equations provided an adequate fit across the range of the data, the three-parameter model (Eq. (4)) followed the measured field data more closely than the Brooks and Corey model (Eq. (5)), primarily for $\psi > -0.3$ MPa. For example, when $\psi = -0.05$ MPa at 20 cm in the OG-PP site, $\theta = 0.077$ m^3 m^{-3} for the three parameter model (closely matching the measured value), but $\theta = 0.091$ m^3 m^{-3} for the Brooks and Corey model (Fig. 1, inset). This discrepancy was a result of constraining θ_s and θ_r to realistic values ($0 < \theta_r < \theta_s < 1$). Unconstrained, the four-parameter model yielded a similar fit to the three-parameter model throughout the range of measured data. Parameter values for each curve are described in Table 2.

Across all sites, deeper soil layers contained more water than shallow layers at a given value of ψ because of distinct depth-dependent changes in soil physical characteristics. For example, when soil $\psi = -0.1$ MPa at the OG-PP site, θ ranged from 0.07 m^3 m^{-3} at 20 cm to 0.19 m^3 m^{-3} at 100 cm. Similarly, when soil $\psi = -0.1$ MPa at the OG-DF site, θ ranged from 0.13 m^3 m^{-3} at 20 cm to 0.35 m^3 m^{-3} at 100 cm (Fig. 1). This two- to three-fold variation in θ at a particular soil ψ was attributable to differences in soil physical characteristics; including soil BD, organic matter, and particle size distribution (see regression analysis below).

Most of the seasonal water use from the upper 1 m at all sites was released before soil ψ reached −0.1 MPa (Fig. 1). Over a 50-day droughty period, 35–60% (Y-DF, increasing % with depth), 50–90% (OG-DF), or 30–75% (OG-PP) of the total soil water uptake occurred before soil ψ reached −0.05 MPa. Relative soil θ in the 15–60 cm layer declined similarly at the Douglas-fir sites during the drying period (50 days), from 0.18–0.28 to 0.10–0.17 $m^3\ m^{-3}$ depending on depth (Fig. 2d and e), releasing 40–45% of its original storage volume. In contrast, at the OG-PP site (which had 110 days of drying), θ in the 15–60 cm layer declined from 0.13–0.23 to 0.05–0.10 $m^3\ m^{-3}$ (Fig. 2f), releasing 52–58% of its original volume. Deep soil (2 m) at the Douglas-fir sites remained relatively moist during this period (0.4 or 0.5 $m^3\ m^{-3}$ for Y-DF and OG-DF soils, respectively), releasing only about 5% of its original volume. Deep soil at the OG-PP site was relatively dry compared to the Douglas-fir sites and released a greater fraction of its stored water, with θ at 2 m declining from 0.29 to 0.24 $m^3\ m^{-3}$ during the seasonal dry-down, releasing about 20% of its original volume.

Water use from the upper 2 m began to decline three weeks (Y-DF) or 6-weeks (OG-DF, OG-PP) after the onset of soil drying (Fig. 2a–c), when average soil ψ ∼−0.3 (Y-DF), ψ ∼−0.1 (OG-DF) or ψ ∼−0.4 (OG-PP) MPa in the 15–30 cm layer. Maximum daily rates of water use varied with the stand, with a maximum of 2.5 mm day^{-1} at the Y-DF, followed by 1.8 at the OG-DF, and 1.3 at the OG-PP. Total daily sap flux density in the OG-DF trees reached a maximum in late June to early July (Fig. 2b), which coincided with the initiation of upper soil drying (Fig. 2e), then sap flux density began to decline 3 weeks later at the onset of the dry period. In contrast, sap flux density of OG-PP trees continued to increase after soil drying began, peaking 6 weeks later (Fig. 2c). Maximum sap flux density in the outer sapwood was similar for all

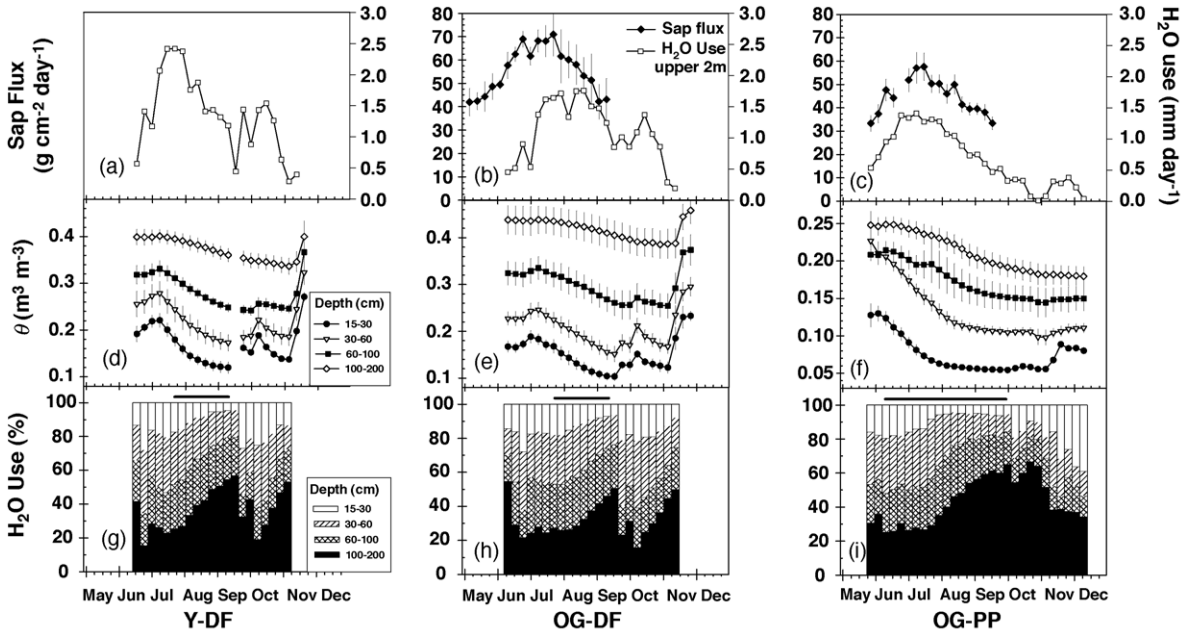

Fig. 2. Seasonal weekly water dynamics for young- and old-growth Douglas-fir stands (Y-DF, OG-DF), and for an old-growth ponderosa pine stand (OG-PP): (a–c) total daily water use from the upper 2 m soil profile based on fluxes in soil volumetric water content. Also depicted (b–c) total daily sap flux density ±S.E. for trees in an old-growth Douglas-fir stand and an old-growth pine stand based on thermal dissipation probes installed 2 cm into sapwood at 2 m height. (d–f) Average seasonal decline in volumetric soil water content by depth ±S.E. (n = 4). (g–i) Relative water use from individual layers in the upper 2 m of the soil profile based on fluxes in soil volumetric water content. Horizontal bars at the top of (g–i) span the 2002 seasonal drought for each stand, and represent the period used for development of the soil water retention curves (Fig. 1).

species at both old-growth sites, ranging from 30–70 g cm^{-2} day^{-1}.

Water extraction shifted to the deeper soil layers as the summer drought progressed. Early in the season (June–July), almost 50% of the water used in the upper 2 m was extracted from the upper 15–60 cm (Fig. 2g–i). At the end of the drought (September–October), only 20% of the water came from the upper 15–60 cm of the profile. This trend was consistent across all sites. The soils began to recharge following late September (Y-DF, OG-DF; Fig. 2d and e) or early November (OG-PP; Fig. 2f) precipitation, at which time water extraction from the upper 15–60 cm returned to 50% (Fig. 2g–i). Only minimal soil water recharge was apparent at the OG-PP site by December (Fig. 2f) when the precipitation began falling as snow.

The initiation of hydraulic redistribution of soil water from deep sources to the upper profile began when water potentials in the upper 60 cm declined to −0.05 to −0.3 MPa, depending on soil type. Initiation of HR was correlated with the droughty period, such that HR began later in the year at the DF sites than at the PP site (Fig. 3). The Y-DF site had a steeper rate of increase in HR than the OG-DF site, which lagged behind by up to 2 weeks even though both sites were exposed to similar precipitation and temperature regimes. Maximum rates of HR were similar among the three sites and approached 0.15 mm day^{-1} in the upper 15–60 cm of the soil profile, which replaced at least 60% of daily depletion in the upper 15–60 cm,

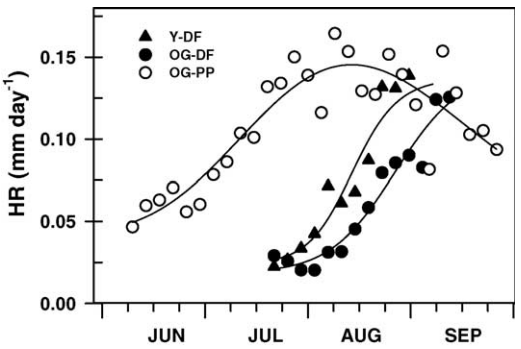

Fig. 3. Hydraulic redistribution (HR) of soil water by roots for young- and old-growth Douglas-fir stands (Y-DF, OG-DF), and for an old-growth ponderosa pine stand (OG-PP) based on diel fluctuations in volumetric soil water content in the upper 15–60 cm during the 2002 drought (Table 1).

until the autumn rains equalized the water potential gradient between the soil layers.

Soil bulk density measured at 20 cm intervals between 10 and 70 cm was 0.84 ± 0.02, 0.96 ± 0.06, 1.01 ± 0.03 g cm^{-3} at Y-DF, 0.81 ± 0.02, 0.76 ± 0.01, 0.79 ± 0.01 g cm^{-3} at OG-DF, and 0.96 ± 0.05, 1.12 ± 0.03, 1.52 ± 0.12 g cm^{-3} at OG-PP. A distinct layer of gravel was present in our 50–70 cm sample at OG-PP, which increased BD and SE. BD increased with depth at the Y-DF site and at the OG-PP site, but not at the OG-DF site. Values were similar to those reported by Klopatek (2002) for the Douglas-fir stands. Prior measurements of BD at the OG-PP site ranged from 1.05–1.23 g cm^{-3} in the upper 100 cm (Law et al., 2001a,b). Modeled values of K_s based on texture, BD, and θ at specific ψ were 14.4, 11.3, 23.4 cm h^{-1} (0–20 cm), 10.9, 15.6, 21.4 cm h^{-1} (20–40 cm), and 7.3, 20.9, 9.3 cm h^{-1} (40–60 cm) for the Y-DF, OG-DF, and OG-PP sites, respectively. Modeled values of K_s based solely on texture were 1.5, 1.5, 3.5 cm h^{-1} (0–20 cm), 1.1, 1.6, 3.4 cm h^{-1} (20–40 cm), and 0.6, 1.7, 2.5 cm h^{-1} (40–60 cm) for the Y-DF, OG-DF, and OG-PP sites respectively, similar to values that can be derived from Campbell (1985).

Modeled K_s was depth-dependent and related to soil texture; K_s was positively correlated with sand (%), and negatively correlated with clay (%).

The Y-DF soil was identified as a sandy loam (0–40 cm), which increased in clay content to a loam (40–60 cm) then decreased in clay content to a loamy sand. The OG-DF soil was confirmed as a sandy loam (0–80 cm) which decreased in clay content into loamy sand at 80–200 cm. Particle size distribution differed significantly between the two DF stands from 20 to 80 cm depths; the Y-DF stand had lower sand, and higher silt and clay content than the OG-DF stand (Fig. 4). Both DF soils had significantly lower sand, and higher silt and clay contents in the upper 60 cm than the OG-PP soil, which transitioned from loamy sand at the surface (0–40 cm) to a sandy loam below 40 cm (Fig. 4). Total root biomass in the upper 1 m was 2.16, 2.83, and 2.04 kg m^{-2} for the Y-DF, OG-DF, and OG-PP sites, respectively, and was not significantly different across the sites ($F = 3.3$, $P = 0.067$), nor were there differences in vertical root distribution between sites when all size classes were combined ($F = 0.7$, $P = 0.52$). However, total fine root biomass in the upper 1 m was significantly higher at the

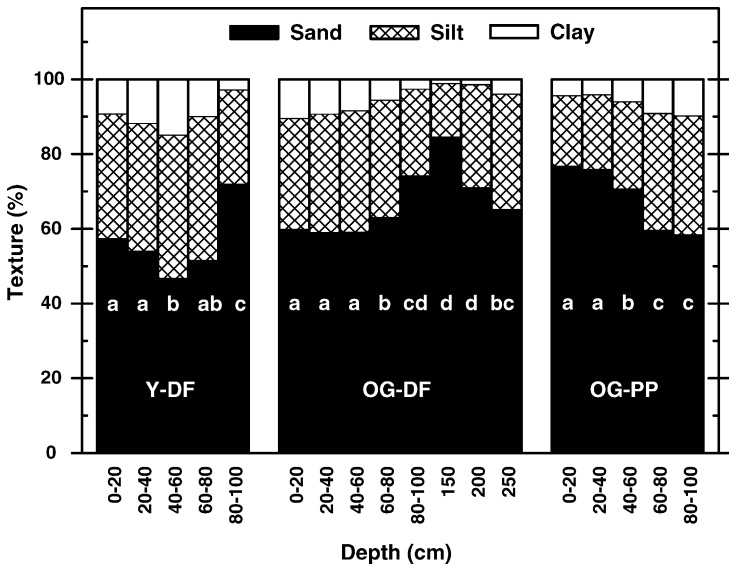

Fig. 4. Soil particle size distribution through the soil profile for young- and old-growth Douglas-fir stands (Y-DF, OG-DF), and for an old-growth ponderosa pine stand (OG-PP). ANOVA and Duncan's multiple range test were used to identify differences between layers within each site (n = 6–8 for depths ≤100 cm, n = 2–4 for depths >100; average S.E. = 0.9% (clay) to 1.8% (sand) for depths ≤100 cm). Soil depths with the same letter within each site were not statistically different in particle size distribution.

Douglas-fir sites, than at the pine site ($F > 2.9$, $P < 0.05$); fine root biomass was 1.15, 1.08, and 0.77 kg m^{-2} for the Y-DF, OG-DF, and OG-PP sites, respectively (Fig. 5). These values are similar to the 0.82 ± 0.14 kg m^{-2} found across 10 studies of various temperate coniferous forests (Jackson et al., 1997). Between 65 and 75% of the fine root biomass in the top 1 m of soil was located in the upper 40 cm at all sites (Fig. 5). The Y-DF site had 15% of fine root biomass located in the organic soil layer (0–4.1 cm) and 36% of fine root biomass in the 4.1–20 cm mineral soil layer. The OG-DF site had over 30% of fine root biomass in the organic soil layer (0–5.8 cm) and 27% of fine root biomass in the 5.8–20 cm mineral soil layer. The OG-PP site had 7% of fine root biomass in the organic soil layer (0–3.5 cm) and 42% of fine root biomass in the 3.5–20 cm mineral soil layer. Depth-dependent patterns were similar for medium root biomass; however, no pattern was detectable for coarse root biomass, possibly due to their infrequent sampling occurrence.

There was significantly more root surface area (SA) (<5 mm) in the upper 20 cm at OG-DF (2.26 m^2 m^{-2}) than at OG-PP (1.43 m^2 m^{-2}), or Y-DF (1.80 m^2 m^{-2}) ($F = 8.1$, $P = 0.002$); however, in the 20–100 cm layer there was lower root SA (<5 mm) at OG-DF (2.52 m^2 m^{-2}) and OG-PP (2.34 m^2 m^{-2}) than at Y-DF (2.95 m^2 m^{-2}) ($F = 3.1$, $P = 0.05$). More than 60% of fine root SA in the top 1 m of soil was located in the upper 40 cm at all sites, with at least 40% located in the top 20 cm (Fig. 6). Total fine root SA was higher at the Douglas-fir sites (3.72–3.79 m^2 m^{-2}), than at the pine site (3.01 m^2 m^{-2}; $F > 7.2$, $P < 0.001$). Total sampled root SA in the upper 1 m for all size classes was 5.10, 5.33, and 4.22 m^2 m^{-2} for the Y-DF, OG-DF and OG-PP sites, respectively, and was significantly different between the two old-growth sites. Fine root SA in the organic layer was significantly higher at OG-DF than at the other sites ($F > 9.3$, $P < 0.005$). Medium root SA in the organic layer was higher at OG-DF than at OG-PP ($F > 3.5$, $P < 0.05$). Fine root SA in the top 20 cm was higher at OG-DF than OG-PP ($F > 7.6$, $P < 0.005$).

The depth-dependent variation in SWRC was explained by differences in root SA, soil BD and particle size distribution. The regression analysis revealed that differences in soil texture accounted for 60% of the variability in θ (Table 3, model A). In the upper 100 cm, at $\psi = -0.1$ MPa, the percentages of sand and clay accounted for 62% of the variation. In the top 60 cm, the percentage of silt alone accounted

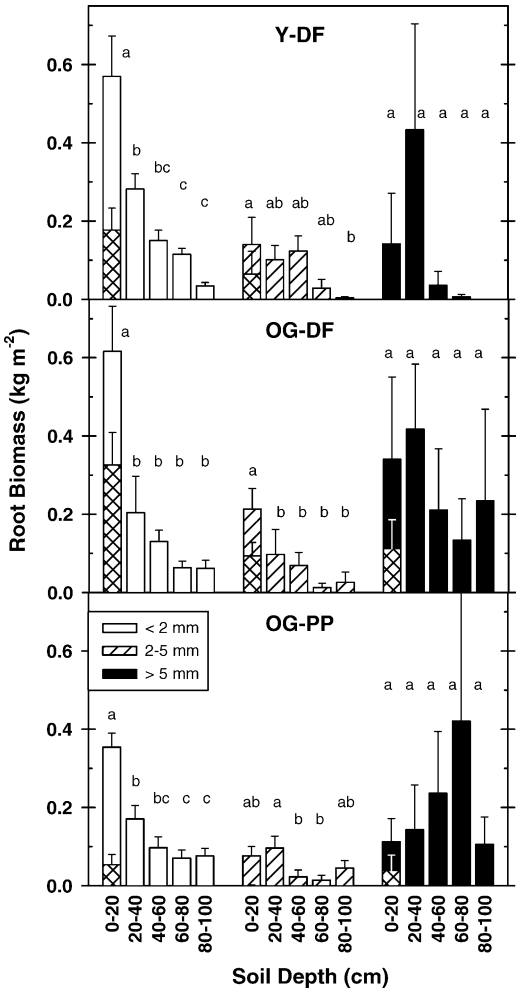

Fig. 5. Root biomass by size class in the upper 1 m for young- and old-growth Douglas-fir stands (Y-DF, OG-DF), and for an old-growth ponderosa pine stand (OG-PP) ($n = 8$, ±1 S.E.). The upper 20 cm layer was divided into the organic and mineral layers; crosshatched bars represent the organic component. Bars with the same letter within each size class are not statistically different based on ANOVA and Duncan's multiple range test ($P < 0.05$).

for 59% of the variation for $-0.1 > \psi > -0.75$ MPa. Inclusion of BD into the model increased the adjusted R^2 of the regression by an additional 3–29% for upper 60 cm (Table 3, model B). Root SA also accounted for significant variation (8–34%) in the SWRC (Table 3, model C), and based on the BIC statistic was a more important component of the complete regression than measured BD (Table 3, model D). Since both BD and root SA change with soil depth, they were significantly correlated ($r = -0.65$) which affected their interaction within the complete regression model (Table 3, model D). As BD increased with depth, root surface area (and root biomass) decreased with depth. Pearson correlation coefficients (r) related depth to root biomass ($r = -0.77$), depth to root surface area ($r = -0.85$), and depth to BD ($r = 0.65$).

In the young stand (Y-DF), maximum rates of water depletion in the upper 2 m of soil (2.5 mm day^{-1}) were greater than those in either the OG-DF (1.8 mm day^{-1}) or OG-PP (1.5 mm day^{-1}) stand, when upper soil ψ was above −1.0 MPa (Fig. 7). For example, when the ψ at 20 cm was −0.5 MPa for all stands, the soil in Y-DF was losing about 2 mm day^{-1} over the entire 2 m of soil, compared to 1.4 mm day^{-1} for both of the older stands (Fig. 7).

At the OG-PP site, total evapotranspiration based on eddy covariance measurements was higher than could be accounted for by water depletion in the upper 2 m, indicating that substantial amounts of water were extracted from depths below 2 m (Fig. 8). Water extracted from below 2 m increased during the drought from 0.4 mm day^{-1} (July) to 0.7 mm day^{-1} (September), even as total site water use declined by 0.6 mm day^{-1}.

4. Discussion

The patterns of seasonal soil water extraction were similar between all sites during the summer drought although the SWRC that described water extraction varied widely between and within sites. More than 40% (PP) to 60% (DF) of fine roots were located in the upper 20 cm of soil; however, the 0–20 cm layer only accounted for 4–20% of the water depletion from the upper 2 m during the seasonal drought, illustrating the large contribution of deeper roots to water uptake. Nevertheless, daily water uptake from the entire 2 m profile was strongly dependent on water potential at 20 cm. This relationship diminished with increasing depth, suggesting that fine roots in the upper soil may play an important role in regulating water uptake through hydraulic or chemical (e.g., abscisic acid) effects on stomatal conductance (Meinzer and Grantz, 1990; Davies et al., 1994; Sperry et al., 1998; Meinzer, 2002).

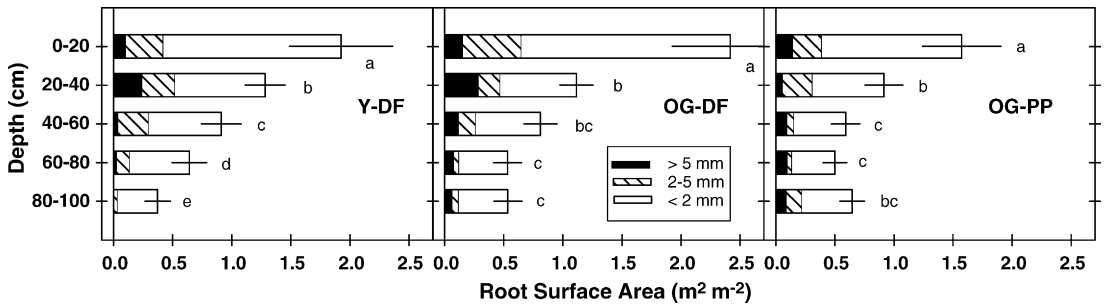

Fig. 6. Total root surface area for young- and old-growth Douglas-fir stands (Y-DF, OG-DF), and for an old-growth ponderosa pine stand (OG-PP) separated by size classes. Bars with the same letter within each site are not statistically different based on ANOVA and Duncan's multiple range test ($P < 0.05$). Error bars represent ±1 S.E. about the mean total root surface area within each depth.

4.1. Soil water retention curves

The SWRC analysis provided a relationship between soil water release and physical and biological characteristics of the soil that may be used for future modeling efforts at similar sites in the Pacific Northwest or other regions with similar soil properties. The regression analysis revealed that soil texture

Table 3
Summary of best-fit multiple linear regression analyses to explain the depth-dependent variation in water content at two specific water potential values

$\psi = -0.10$ MPa						$\psi = -0.75$ MPa					
Model	n	R^2_{adj}	F	Pr > F	BIC	Model	n	R^2_{adj}	F	Pr > F	BIC
A	13	0.62	10.9	0.0031	−72.18	A	10	0.59	14.1	0.0056	−69.91
B	11	0.65	10.3	0.0061	−73.76	B	10	0.88	22.0	0.0012	−77.46
C	13	0.70	10.3	0.0028	−72.99	C	10	0.93	60.2	<0.0001	−85.04
D	11	0.82	23.2	0.0005	−79.14	D	10	0.93	60.2	<0.0001	−84.71

Model	Parameter	Parameter estimate	S.E.	t	Pr > $\|t\|$	Model	Parameter	Parameter estimate	S.E.	t	Pr > $\|t\|$
A	Sand	−2.60E−02	5.71E−03	−4.55	0.0011	A	Silt	4.31E − 03	1.15E − 03	3.76	0.0056
	Clay	−7.11E−02	1.52E−02	−4.67	0.0009		Intercept	−1.89E − 03	3.32E − 02	−0.06	0.956
	Intercept	2.39E+00	4.78E−01	4.99	0.0005						
B	Silt	6.11E−03	1.35E−03	4.53	0.0019	B	Sand	2.09E − 02	6.84E − 03	3.05	0.0225
	BD	1.26E−01	6.59E−02	1.92	0.0917		Silt	3.76E − 02	1.05E − 02	3.59	0.0115
	Intercept	−1.39E−01	8.65E−02	−1.61	0.1462		BD	2.49E − 01	5.61E − 02	4.45	0.0043
							Intercept	−2.51E + 00	7.65E − 01	−3.28	0.0168
C	Sand	−2.14E−02	5.63E−03	−3.80	0.0042	C, D	Sand	−3.32E − 03	3.29E − 04	−10.09	<0.0001
	Clay	−5.59E−02	1.58E−02	−3.54	0.0063		SA_{root}	−8.58E − 02	1.35E − 02	−6.37	0.0004
	SA_{root}	−1.06E−01	5.61E−02	−1.89	0.0909		Intercept	4.12E − 01	2.69E − 02	15.33	<0.0001
	Intercept	2.07E+00	4.58E−01	4.52	0.0014						
D	Sand	−3.79E−03	6.20E−04	−6.12	0.0003						
	SA_{root}	−9.20E−02	2.41E−02	−3.82	0.0051						
	Intercept	4.82E−01	4.79E−02	10.07	<0.0001						

Four models were used: (A) $\theta \approx$ sand + silt + clay, (B) $\theta \approx$ sand + silt + clay + bulk density (BD), (C) $\theta \approx$ sand + silt + clay + root surface area (SA_{root}), (D) $\theta \approx$ sand + silt + clay + BD + SA_{root} (see text description). Soil water retention curves from all three study sites were used in the analysis (Fig. 1). Missing BD and θ (at $\psi = -0.75$ MPa) at 100 cm depth reduced the sample size, thus for $n < 11$, modeled depth ≤60 cm. Models used the best-fit adjusted R^2 selection technique and included the Bayesian information criterion statistic (BIC) to compare different models. Higher absolute values of BIC indicate a better regression model.

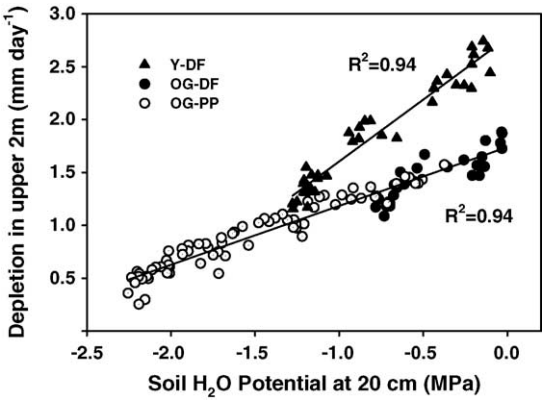

Fig. 7. Daily water depletion from the upper 2 m of soil at the three study sites in response to the water potential of the upper soil. Linear regression curves were fit for the young site or for the two old-growth sites together.

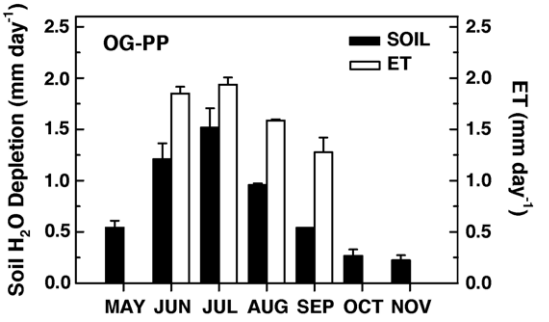

Fig. 8. Seasonal water loss from the old-growth ponderosa pine stand (OG-PP) based on volumetric soil water depletion in the upper 2 m of soil (soil H_2O deletion), or on eddy covariance measurements of site water vapor flux from a 47 m tower (evapotranspiration, ET). Soil water depletion was measured during 2002 and 2003. Eddy covariance measurements were made during 1996–1997 (Law et al., 2000a) and 2000 (Anthoni et al., 2002). Error bars represent the S.E. between years (n = 2–3).

was the most important component affecting vertical gradients of in situ soil water release accounting for about 60% of the variation (Table 3). Soil texture affects soil pore space size which is inextricably linked to ψ and θ and is the main element of most pedotransfer functions (e.g., Saxton et al., 1986; Wösten et al., 2001). The addition of BD to knowledge of soil particle size distribution (sand, silt, clay (%)) could be used to produce a linear pedotransfer function, accounting for 65–88% of the variability in water release under drying conditions. A pedotransfer function incorporating particle size distribution and root surface area provided better results (70–93%), although BD is easier to characterize and more likely to be available than root surface area. Soil organic matter (SOM) also has a strong effect on water retention (Rawls et al., 2003) and could contribute to future analyses if vertical gradients in SOM are quantified. The OG-PP pine site had much lower SOM than the DF sites resulting in lower θ for a specific ψ throughout the vertical soil profile. SOM was correlated with fine root biomass and depth; declining from high levels in the organic mull layer to progressively lower levels into the mineral soil (see Section 2.1).

The three-parameter SWRC provided the best site-specific fit to in situ water retention; however, other models (e.g., Brooks and Corey) whose parameters describe physical characteristics of the soil may also provide an adequate representation of soil water retention. Consideration should be given to model errors that arise during the transitional phase in the SWRC, where small changes in ψ result in increasingly large changes in θ (Fig. 1b inset). This transitional phase corresponds to the period of upper soil drying, the initiation of HR, the downward shift in relative water uptake, and the time when water status of the upper soil may begin to influence stomatal conductance. Thus, the relatively small shift observed between the two types of SWRC equations, may scale up to larger predicted effects on water fluxes in ecosystem level models that incorporate estimates of soil water release (e.g., Sperry et al., 1998).

4.2. Root water uptake and transport

Roots continued to deplete water in the upper soil throughout the drought as available water diminished and water potentials approached −1 MPa (DF) or −2 MPa (PP). Field-measured loss of hydraulic conductivity by medium roots (2–4 mm) in the upper soil at all three sites never exceeded 50% during the dry season (Domec et al., 2004), even as their contribution to water uptake dropped below 10%. Hydraulic conductivity of roots from the same cohort measured after autumn rainfall events had recovered to their pre-drought values, which ranged from 20 to 30% loss of conductivity—the apparent native operating conductivity for these roots under moist

conditions (Domec et al., 2004). Roots have been shown to lose conductivity earlier than stems during a drought (Hacke et al., 2000), which may generate a hydraulic or chemical signal to regulate stomatal conductance (Meinzer and Grantz, 1990; Sperry et al., 1998; Meinzer, 2002; Domec et al., 2004).

The initiation of hydraulic redistribution coincided with the transitional phase in the SWRC where small declines in θ resulted in large declines in ψ. Even though HR represented just a fraction (5–10%) of total water use from the upper 2 m during this transitional phase, the daily partial recharge of upper θ by HR was enough to slow the decline in soil ψ and thus maintain upper soil water availability. Towards the end of the drought, nighttime HR of soil water from deeper layers replaced 0.15 mm day^{-1} in the upper soil (15–60 cm), which represented 60–80% of the water extracted from that layer each day. This influx of soil water thus slowed the decline in soil ψ, thereby delaying increased root xylem embolism and extending root function later into the drought (Domec et al., 2004). It may be beneficial for the plant to maintain some hydraulic conductivity in upper roots during droughty periods to allow continued uptake of nutrients essential for growth and maintenance from the relatively nutrient-rich upper soil layers (Caldwell et al., 1998), especially in forest ecosystems that are often nutrient limited. Even in the absence of precipitation, hydraulically redistributed water released into the rhizosphere could partially maintain the availability of soil solution for uptake by roots if their hydraulic conductivity has also been maintained above a critical threshold. The rapid increase in root water uptake from the upper soil following late September rainfall events (Fig. 2g–i) suggested that complete root xylem dysfunction had been avoided in the upper soil or that embolism reversal in shallow roots was rapid following partial rewetting of the soil (Domec et al., 2004).

Water uptake is not limited to the region near the tips of white fine roots, but can occur at similar rates for older, visibly brown, suberizing root sections as demonstrated for *Pinus elliotii* Engelm. seedlings (van Rees and Comerford, 1990). Medium and coarse woody roots (>2 mm) accounted for a significant portion of sampled root biomass in this study, especially at deeper depths where fewer fine roots were sampled. However, coarse roots have only a fraction of the water-absorbing surface area of the finer roots, whose rate of water uptake in the field has been shown to be an order of magnitude greater than that of coarse roots (J. Lindenmair, personal communication). Even so, in addition to their role in structural support and water transport, coarse woody roots can take up significant amounts of water, as demonstrated for 0.2–5 cm diameter roots of several mature woody species (Lindenmair et al., 2004). The potential contribution of coarse woody roots to root SA, and thus water uptake is likely underestimated in this study due to a low frequency of occurrence in sampled soil cores, large variations in size, an often vertical orientation (necessary for transporting water from depth), and the existence of unsampled roots below 1 m.

4.3. Vertical variation in water uptake

Patterns of root water uptake were surprisingly similar, regardless of site, species or age of trees. Between 47–80% (Y-DF), 53–77% (OG-DF) and 48–84% of the water uptake from the upper 2 m during the droughty period was extracted from depths below 60 cm (Fig. 2g–i), where there was less than 25% of measured root area. This suggests that either the majority of total root surface area was not sampled (i.e., that most root surface area existed below 1 m), or that the rate of root water uptake per area is greater at depth—where higher water availability ($\psi > -0.3$ MPa) dramatically reduces uptake resistance. Burgess et al. (2000) also found that significant water uptake from depth occurred seasonally in *Banksia prionotes* Lindl. based on sap flux measurements in roots and trunks. In agreement with our observations, they found that water uptake progressed to deeper layers as the soils dried during the summer drought, and then shifted back to shallow layers as precipitation penetrated the upper soils. Bréda et al. (1995) found similar shifts in water uptake seasonally by oak roots (*Quercus* sp.).

As water depletion from the upper 2 m in the OG-PP site decreased, water uptake by deeper roots necessarily increased by more than 50% to account for the differences between measured soil water loss and evapotranspiration (Fig. 8). Only about 80% of maximal site water use (July) was accounted by soil water depletion in the upper 2 m. This proportion declined to 60% in August and then to 40% by

September due to reduced soil water availability in the upper profile under drying conditions. Water potential of the upper soil (20 cm) and tree foliage (mid-day; data not shown) approached −2 MPa toward the end of the drought at the OG-PP site while the minimum measured soil ψ in the deeper soil (1 m) was −0.4 MPa. Thus the ψ below 2 m was likely closer to zero. The resulting ∼2 MPa ψ gradient acted as the driving force for water transport from deep soil to the tree foliage.

4.4. Site differences in water uptake

The two Douglas-fir stands had more stored water in the upper 2 m during the drought than the pine stand, which resulted in smaller soil–leaf ψ gradients—even under similar environmental conditions. It is not known if total site evapotranspiration differed between the DF and PP sites, or between the young and old DF stands, although recent eddy covariance data for the DF stands shows maximum daily water use peaking at 1.7–3.0 mm day^{-1} (Unsworth et al., 2004; Chen et al., 2004), which overlaps with the reported 1.8–2.1 mm day^{-1} rates of water use at the PP site (Law et al., 2000a; Anthoni et al., 2002). Higher daily transpiration was estimated for younger forests in several studies that compared water use in young and old-growth Douglas-fir forests using stem sap flux measurements that were scaled up to the canopy level (Phillips et al., 2002; Moore et al., 2004). The more rapid uptake of soil water at Y-DF as compared with OG-DF (Fig. 2a and b) and the higher total rates of depletion at Y-DF (Fig. 7) are consistent with the hypothesis that young DF stands may use more water than older stands under similar conditions, although mixed results have been reported based on eddy covariance measurements in different aged Douglas-fir stands (Chen et al., 2004). The relationship for both old-growth stands between total water depletion from the upper 2 m and soil ψ at 20 cm fell along the same regression line, with decreasing soil ψ having a much smaller effect on water depletion in the old-growth stands than in the young stand until soil ψ reached ∼−1.25 MPa at which point all three stands had similar rates of daily soil water depletion. If soil ψ at 20 cm in the young stand had fallen below −1.25 MPa during the study period, it is possible that the relationship between soil water depletion and soil ψ would have begun to follow the same trajectory as in the old-growth stands.

The greater responsiveness of soil water depletion to soil ψ in the young stand may have been associated with differences in the vertical distribution of root surface area (SA_{root}) in the young and old-growth stands. The higher root SA sampled in the deeper, moister soil (20–100 cm) at Y-DF would allow a mechanism for the higher rates of water uptake exhibited by the young stand as compared with the two older stands (Fig. 2a–c). The sharper decline in water use with declining soil ψ for the young stand (Fig. 7) may be attributable to its developmental age and stand density, reflecting the dynamics of site exploration and competition for resources. Trees in the older stands have had hundreds of years of soil exploration and root turnover that in turn affected soil structure, resource availability, and ultimately stand functional stability. The more even vertical distribution with depth of roots in the older stands may have led to a relatively buffered response of total soil water depletion to upper soil water potential. It is notable that even with differences in species, stand density, basal area, leaf area (Table 1), soils and climate, soil water utilization in the two old-growth stands behaved more similarly than in the two different-aged Douglas-fir stands located on similar sites exposed to nearly identical climate regimes.

4.5. Regulation of water uptake

Our results indicate that during the growing season, absolute water use was not limited by water availability at depth for either DF or PP sites, but rather by interactions between pathway resistances and ψ driving forces induced above 2 m. Apparent rhizosphere conductance and water utilization in the upper 20–60 cm of soil shared a common linear relationship across all sites, but site-specific linear relationships developed when relating water utilization of the entire 2 m profile to rhizosphere conductance in the 20–60 cm layer (Meinzer et al., 2004). These relationships are likely related to differences in root distribution and soil physical characteristics that affect the water retention through the profile at each site.

Soil ψ at a single depth (20 cm) was a good predictor of total daily water depletion from the upper 2 m at all sites (Fig. 7). Daily water uptake by roots is governed largely by transpiration, which in turn is

regulated by integrated stomatal responses to external environmental variables such as vapor pressure deficit and irradiance as well as internal hydraulic (Meinzer and Grantz, 1990; Sperry et al., 1998; Meinzer, 2002) and chemical (i.e., abscisic acid; ABA) signals (Davies et al., 1994). A hydraulic signal could cause leaf ψ to decline enough to affect release of stored leaf ABA, and thereby reduce stomatal conductance. It is also possible that ABA generated in the roots and transported through the xylem to the leaf acts as a chemical signal that may be proportional to soil water status (Tardieu et al., 1991; Davies et al., 1994) or loss of root hydraulic conductivity (Domec et al., 2004). Either way, stomatal responses to drying in the uppermost soil layers appeared to regulate water uptake in the upper 2 m in a consistent manner across all of the study sites (Fig. 7). Some models such as the soil-plant-atmosphere model of canopy processes (SPA) incorporate this connection between soil properties and leaf conductance into the model (Williams et al., 1996).

5. Conclusions

Knowledge of the predictable, non-linear release of soil water for plant uptake is critical for modeling soil water fluxes at the landscape level. This work illustrates the potential error in curve equations used to relate θ and ψ and to model water release. Seasonal depletion of stored water shifted downward as the soils dried, illustrating the vertical stratification of soil physical and biological components. Although root distribution was weighted toward the nutrient rich upper soil, most water uptake occurred at depths greater than 60 cm where deeper roots accounted for 50–80% of water uptake under drying conditions. Accurate modeling of water flux through forested ecosystems must take into account vertical stratification and seasonal dynamics of soil water release, and the causal soil physical and biological characteristics.

Acknowledgements

This research was supported by the USDA Forest Service Ecosystem Processes Program, the US Environmental Protection Agency, and the Wind River Canopy Crane Research Facility located within the Wind River Experimental Forest, T.T. Munger Research Natural Area in Washington State, USA. The facility is a cooperative scientific venture among the University of Washington, the USDA Forest Service Pacific Northwest Research Station and Gifford Pinchot National Forest. This manuscript has been subjected to the Environmental Protection Agency's peer and administrative review, and it has been approved for publication as an EPA document. Mention of trade names or commercial products does not constitute endorsement or recommendation for use. We thank Ken Bible and Bev Law for providing site data, John Selker for discussion, Pat Cunningham for statistical consultation, and David Woodruff, Abby Burnett, Rob Coulombe, Heather Nagel and Hollie Oakes-Miller for fieldwork and data analysis.

References

Abrahamson, D.A., Dougherty, P.M., Zarnoch, S.J., 1998. Hydrological components of a young loblolly pine plantation on a sandy soil with estimates of water use and loss. Water Resour. Res. 34, 3503–3513.

Anthoni, P.M., Unsworth, M.H., Law, B.E., Irvine, J., Baldocchi, D.D., Van Tuyl, S., Moore, D., 2002. Seasonal differences in carbon and water vapor exchange in young and old-growth ponderosa pine ecosystems. Agric. Forest Meteorol. 111, 203–222.

Bréda, N., Granier, A., Barataud, F., Moyne, C., 1995. Soil water dynamics in an oak stand I. Soil moisture, water potential and water uptake by roots. Plant Soil 172, 17–27.

Brooks, J.R., Meinzer, F.C., Coulombe, R., Gregg, J., 2002. Hydraulic redistribution of soil water during summer drought in two contrasting Pacific Northwest coniferous forests. Tree Physiol. 22, 1107–1117.

Brooks, J.R., Meinzer, F.C., Warren, J.M., Domec, J.-C., Coulombe, R., in review. Hydraulic redistribution in a Douglas-fir forest: lessons from system manipulations. Plant Cell Environ.

Brooks R.H., Corey A.T., 1964. Hydraulic properties of porous media. Hydrology Paper no. 3. Civil Engineering Department, Colorado State University.

Brown R.W., Bartos D.L., 1982. A calibration model for screen-caged Peltier thermocouple psychrometers. USDA Forest Serv. Res. Pa INT-293. Intermt. Forest Range Exp. Stn., Ogden, UT

Bucci, S.J., Goldstein, G., Meinzer, F.C., Scholz, F.G., Franco, A.C., Bustamante, M., 2004. Functional convergence in hydraulic architecture and water relations of tropical savanna trees: from leaf to whole plant. Tree Physiol. 24, 891–899.

Burgess, S.S.O., Pate, J.S., Adams, M.A., Dawson, T.E., 2000. Seasonal water acquisition and redistribution in the Australian woody phreatophyte, *Banksia prinotes*. Ann. Bot. 85, 215–224.

Caldwell, M.M., Dawson, T.E., Richards, J.H., 1998. Hydraulic lift: consequences of water efflux from the roots of plants. Oecologia 113, 151–161.

Campbell, G.S., 1985. Soil Physics With Basic; Transport Models for Soil–Plant Systems. Elsevier, Amsterdam.

Chen, J., Paw, U.K.T., Ustin, S.L., Suchanek, T.H., Bond, B.J., Brosofske, K.D., Falk, M., 2004. Net ecosystem exchanges of carbon, water, and energy in young and old-growth Douglas-fir forests. Ecosystems 7, 534–544.

Childs, S.W., Hanks, R.J., 1975. Model of soil salinity effects on crop growth. Soil Sci. Soc. Am. Proc. 39, 617–623.

Clearwater, M.J., Meinzer, F.C., Andrade, J.L., Goldstein, G., Holbrook, N.M., 1999. Potential errors in measurement of non-uniform sap flow using heat dissipation probes. Tree Physiol. 19, 681–687.

Davies, W.J., Tardieu, F., Trejo, C.L., 1994. How do chemical signals work in plants that grow in drying soil? Plant Physiol. 104, 309–314.

Dean-Knox, D.E., Devitt, D.A., Verchick, L.S., Morris, R.L., 1998. Physiological response of two turfgrass species to varying ratios of soil matric and osmotic potentials. Crop Sci. 38, 175–181.

Domec, J.-C., Warren, J.M., Meinzer, F.C., Brooks, J.R., Coulombe, R., 2004. Native root xylem embolism and stomatal closure in stands of Douglas-fir and ponderosa pine: mitigation by hydraulic redistribution. Oecologia 141, 7–16.

Donovan, L.A., Richards, J.H., Linton, M.J., 2003. Magnitude and mechanisms of disequilibrium between predawn plant and soil water potentials in desert shrubs. Ecology 84, 463–470.

Gee, G.W., Bauder, J.W., 1986. Particle-size analysis. In: Page, A.L. (Ed.), Methods of soil analysis. Part 1. Physical and mineralogical methods. Agronomy Monograph 9, second ed. American Society of Agronomy, Madison, WI. pp. 383–411.

Granier, A., 1985. Une nouvelle méthode pour la mesure de flux de sčve brute dans le tronc des arbres. Ann. Sci. Forest 42, 193–200.

Hacke, U.G., Sperry, J.S., Ewers, B.E., Ellsworth, D.S., Schäfer, K.V.R., Oren, R., 2000. Influence of soil porosity on water use in *Pinus taeda*. Oecologia 124, 495–505.

Heiskanen, J., Mäkitalo, K., 2002. Soil water-retention characteristics of Scots pine and Norway spruce forest sites in Finnish Lapland. Forest Ecol. Manage. 162, 137–152.

Irvine, J., Law, B.E., Anthoni, P.M., Meinzer, F.C., 2002. Water limitations to carbon exchange in old-growth and young ponderosa pine stands. Tree Physiol. 22, 189–196.

Jackson, R.B., Mooney, H.A., Schulze, E.-D., 1997. A global budget for fine root biomass, surface area, and nutrient contents. Proc. Natl. Acad. Sci. U.S.A. 94, 7362–7366.

James, S.A., Clearwater, M.J., Meinzer, F.C., Goldstein, G., 2002. Heat dissipation sensors of variable length for the measurement of sap flow in trees with deep sapwood. Tree Physiol. 22, 277–283.

Katul, G., Todd, P., Pataki, D., Kabala, Z.J., Oren, R., 1997. Soil water depletion by oak trees and the influence of root water uptake on the moisture content spatial statistics. Water Resour. Res. 33, 611–623.

Klopatek, J.M., 2002. Belowground carbon pools and processes in different age stands of Douglas-fir. Tree Physiol. 22, 197–204.

Law, B.E., Goldstein, A.H., Anthoni, P.M., Unsworth, M.H., Panek, J.A., Bauer, M.R., Fracheboud, J.M., Hultman, N., 2001a. Carbon dioxide and water vapor exchange by young and old ponderosa pine ecosystems during a dry summer. Tree Physiol. 21, 299–308.

Law, B.E., Thornton, P.E., Irvine, J., Anthoni, P.M., van Tuyl, S., 2001b. Carbon storage and fluxes in ponderosa pine forests at different developmental stages. Global Change Biol. 7, 755–777.

Law, B.E., Ryan, M.G., Anthoni, P.M., 1999. Seasonal and annual respiration of a ponderosa pine ecosystem. Global Change Biol. 5, 169–182.

Law, B.E., Waring, R.H., Anthoni, P.M., Aber, J.D., 2000a. Measurements of gross and net ecosystem productivity and water vapour exchange of a *Pinus ponderosa* ecosystem, and an evaluation of two generalized models. Global Change Biol. 6, 155–168.

Law, B.E., Williams, M., Anthoni, P.M., Baldocchi, D.D., Unsworth, M.H., 2000b. Measuring and modeling seasonal variation of carbon dioxide and water vapour exchange of a *Pinus ponderosa* forest subject to soil water deficit. Global Change Biol. 6, 613–630.

Licata J., 2003. Structural and physiological changes with stand age: use of a process-based model to compare carbon and water fluxes in young and old-growth Douglas-fir/western hemlock forest stands. Masters Thesis. Department of Forest Science, Oregon State University

Lindenmair, J., Matzner, E., Zimmermann, R., 2004. The role of woody roots in water uptake of mature spruce, beech, and oak trees. In: Matzner, E. (Ed.), Biogeochemistry of Forested Catchments in a Changing Environment—a German Case Study. Springer-Verlag, pp. 279–290.

Meinzer, F.C., 2002. Co-ordination of vapour and liquid phase water transport properties in plants. Plant Cell Envron. 25, 265–274.

Meinzer, F.C., Brooks, J.R., Bucci, S., Goldstein, G., Scholz, F.G., Warren, J.M., 2004. Converging patterns of uptake and hydraulic redistribution of soil water in contrasting woody vegetation types. Tree Physiol. 24, 919–928.

Meinzer, F.C., Grantz, D.A., 1990. Stomatal and hydraulic conductance in growing sugarcane: stomatal adjustment to water transport capacity. Plant Cell Envron. 13, 383–388.

Moore, G.W., Bond, B.J., Jones, J.A., Phillips, N., Meinzer, F., 2004. Structural and compositional controls on transpiration in 40- and 450-year-old riparian forests in western Oregon, USA. Tree Physiol. 24, 481–491.

Morgan, K.T., Parsons, L.R., Wheaton, T.A., Pitts, D.J., Obreza, T.A., 1999. Field calibration of a capacitance water content probe in fine sand soils. Soil Sci. Soc. Am. J. 63, 987–989.

Mualem, Y., 1976. A new model for predicting the hydraulic conductivity of unsaturated porous media. Water Resour. Res. 12, 513–522.

Paltineanu, I.C., Starr, J.L., 1997. Real-time soil water dynamics using multisensor capacitance probes: laboratory calibration. Soil Sci. Soc. Am. J. 61, 1576–1585.

Phillips, N., Bond, B.J., McDowell, N.G., Ryan, M.G., 2002. Canopy and hydraulic conductance in young, mature and old Douglas-fir trees. Tree Physiol. 22, 205–211.

Rawls, W.J., Pachepsky, Y.A., Ritchie, J.C., Sobecki, T.M., Bloodworth, H., 2003. Effect of soil organic carbon on soil water retention. Geoderma 116, 61–76.

Richards, J.H., Caldwell, M.M., 1987. Hydraulic lift: substantial nocturnal water transport between soil layers by *Artemisia tridentata* roots. Oecologia 73, 486–489.

Ryan, M.G., Bond, B.J., Law, B.E., Hubbard, R.M., Woodruff, D., Cienciala, E., Kucera, J., 2000. Transpiration and whole-tree conductance in ponderosa pine trees of different heights. Oecologia 124, 553–560.

Saxton, K.E., Rawls, W.J., Romberger, J.S., Papendick, R.I., 1986. Estimating generalized soil-water characteristics from texture. Soil Sci. Soc. Am. J. 50, 1031–1036.

Schaap, M.G., Leij, F.J., van Genuchten, M.Th., 2001. ROSETTA: a computer program for estimating soil hydraulic parameters with hierarchical pedotransfer functions. J. Hydrol. 251, 163–176.

Schleiff, U., Schaffer, G., 1984. The effect of decreasing soil osmotic and soil matric water potential in the rhizosphere of a loamy and sandy soil on the water uptake rate of wheat roots. Zeitschrift fur Acker- und Pflanzenbau 153, 373–384.

Shaw, D.C., Franklin, J.F., Bible, K., Klopatek, J., Freeman, E., Greene, S., Parker, G.G., 2004. Ecological setting of the wind river old-growth forest. Ecosystems 7, 427–439.

Sperry, J.S., Adler, F.R., Campbell, G.S., Comstock, J.P., 1998. Limitation of plant water use by rhizosphere and xylem conductance: results from a model. Plant Cell Envron. 21, 347–359.

Tardieu, F., Katerji, N., Bethenod, O., Zhang, J., Davies, W.J., 1991. Maize stomatal conductance in the field: its relationship with soil and plant water potentials, mechanical constraints and ABA concentration. Plant Cell Envron. 14, 121–126.

Unsworth, M.H., Phillips, N., Link, T., Bond, B., Falk, M., Harmon, M., Hinckley, T., Marks, D., Paw, U.K.T., 2004. Components and controls of water flux in an old-growth Douglas-fir-western hemlock ecosystem. Ecosystems 7, 468–481.

van Genuchten, M.Th., 1980. A closed-form equation for predicting the hydraulic conductivity of unsaturated soils. Soil Sci. Soc. Am. J. 44, 892–898.

van Rees, K.C.J., Comerford, N.B., 1990. The role of woody roots of slash pine seedlings in water and potassium absorption. Can. J. Forest Resour. 20, 1183–1191.

Williams, M., Rastetter, E.B., Fernandes, D.N., Goulden, M.L., Wofsy, S.C., Shaver, G.R., Melillo, J.M., Munger, J.W., Fan, S.-M., Nadelhoffer, K.J., 1996. Modeling the soil-plant-atmosphere continuum in a *Quercus-Acer* stand at Harvard forest: the regulation of stomatal conductance by light, nitrogen and soil/plant hydraulic properties. Plant Cell Envron. 19, 911–927.

Wösten, J.H.M., Pachepsky, Y.A., Rawls, W.J., 2001. Pedotransfer functions: bridging the gap between available basic soil data and missing soil hydraulic characteristics. J. Hydrol. 251, 123–150.

Yang, S.J., de Jong, E., 1971. Effect of soil water potential and bulk density on water uptake patterns and resistance to flow of water in wheat plants. Can. J. Soil Sci. 51, 211–220.

Zhang, J., Davies, W.J., 1989. Abscisic acid produced in dehydrating roots may enable the plant to measure the water status of the soil. Plant Cell Envron. 12, 73–81.